Bioelectrochemistry 170 (2026) 109261

Contents lists available at ScienceDirect

Bioelectrochemistry

journal homepage: www.journals.elsevier.com/bioelectrochemistry

A porous PEDOT:PSS-cyanobacteria biohybrid for electrochemical assessment of photosynthetic activity☆

Paulo R.F. Rocha [a,*], Raquel Amaral [a], David M.S. Silva [a], Felipe L. Bacellar [a], Luís Lopes [b], Rupert Perkins [c]

[a] Centre for Functional Ecology, Laboratory Associate TERRA, Department of Life Sciences, University of Coimbra, 3000-456 Coimbra, Portugal
[b] Laboratory of Instrumentation and Experimental Particle Physics, Coimbra 3004-516, Portugal
[c] School of Earth and Ocean Sciences, Cardiff University, Cardiff CF10 3AT, United Kingdom

ARTICLE INFO

Keywords:
Cyanobacteria
PEDOT:PSS
Photosynthetic biohybrid
Open-circuit potential
Photocurrent
Environmental monitoring

ABSTRACT

Cyanobacteria are both an emerging platform in sustainable biotechnology, whilst also potentially harmful to water quality in lakes and reservoirs. In both cases, it is surprising that assessment of productivity and abundance still rely upon invasive and often costly and laborious techniques. In this work we devised a biohybrid platform which continuously monitors photosynthetic activity in cyanobacteria, non-invasively and effortlessly. The biohybrid consists of ensembles of *Oscillatoria* sp. adherent on porous poly (3,4-ethylenedioxythiophene) polystyrene sulfonate (PEDOT:PSS) electrodes, which functions as an efficient interface for transducing photosynthetic electron exchange. Open Circuit Potential (OCP) recordings over time were found proportional to the natural light-dark cycles while chronoamperometry revealed light-driven photocurrents absent in abiotic controls. Moreover, cross-correlation analysis between temperature and OCP revealed a distinct phase shift and latency when *Oscillatoria* sp. colonized the electrode, as opposite to medium-only controls, ascertaining a strong biological contribution beyond thermal effects. Overall, this work cements PEDOT:PSS electrodes as a scalable, label-free tool for assessing cyanobacteria photosynthetic activity enabling affordable and continuous water quality monitoring.

1. Introduction

Cyanobacteria are increasingly recognized as valuable platforms for sustainable biotechnology, producing biofuels, chemicals, and high-value compounds through photosynthesis [1–3]. Assessing their productivity accurately and in real time is critical for both laboratory optimization and industrial cultivation. However, conventional methods such as optical density measurements, metabolite assays or chlorophyll fluorescence are typically invasive, indirect and slow, and are poorly suited for continuous monitoring [4].

Beyond biotechnological applications, cyanobacteria are also a major concern in the water industry, where they can produce metabolites responsible for poor water quality (e.g. geosmin and 2-MIB) as well as harmful algal blooms (HABs) that may also release toxins, disrupt ecosystems, and compromise drinking water safety [5]. Existing monitoring approaches such as microscopy, pigment analysis, or molecular methods, are labour-intensive and offer limited temporal or spatial resolution with considerable costs and sampling effort. Additionally, current in situ monitoring does not provide the information needed by lake and reservoir managers, being largely restricted to biomass proxies. There is therefore a pressing need for real-time, non-invasive sensing technologies that can provide dynamic information on cyanobacterial activity, with relevance both to engineered cultivation systems e.g. bioreactors, and to environmental monitoring of cyanobacterial metabolite production and HABs.

Bioelectronic approaches offer a promising alternative by directly coupling microbial activity to electrical signals. Conducting polymers such as poly(3,4-ethylenedioxythiophene): polystyrene sulfonate (PEDOT:PSS) provide a biocompatible, porous, and mixed ionic-electronic conductive matrix that can interface with living cells [6,7]. PEDOT:PSS has been employed in microbial fuel cells [6] and biosensors [8,9], and more recently explored as a transducer in photosynthetic biohybrids [10]. Owing to its large volumetric capacitance and intrinsically low interfacial impedance, PEDOT:PSS provides efficient

☆ This article is part of a Special issue entitled: 'Photobioelectrochemistry' published in Bioelectrochemistry.

* Corresponding author.
E-mail address: procha@uc.pt (P.R.F. Rocha).

https://doi.org/10.1016/j.bioelechem.2026.109261
Received 5 November 2025; Received in revised form 21 January 2026; Accepted 25 February 2026
Available online 26 February 2026

electronic transduction of redox processes at the cell-electrode interface.

In the environmental monitoring of cyanobacterial blooms, many studies use specific cell-density thresholds to flag elevated risk. For example, the WHO recreational water guidelines use ~100,000 cells/mL to define moderate health risk levels associated with cyanobacteria presence [5]. Other studies report bloom events when cell densities approach or exceed 10^7 cells/mL, particularly in dense, persistent bloom scenarios [11,12]. A monitoring method that reliably detects activity at or before these higher densities could therefore serve as an early warning tool, enabling timely intervention in both natural waters and engineered systems.

Here, we present a photosynthetic biohybrid platform in which cyanobacteria adhere and grow within porous PEDOT:PSS electrodes, enabling non-invasive, real-time monitoring of productivity. Using *Oscillatoria* sp. as a model system, we show that porous PEDOT:PSS can report photosynthetic activity through open-circuit potential oscillations and photocurrents, while distinguishing biological contributions from abiotic thermal effects. These findings establish PEDOT:PSS-based biohybrids as effective transducers of cyanobacterial activity, with potential applications in algal biotechnology, bioenergy, and environmental monitoring.

2. Materials and methods

2.1. Fabrication of porous PU/PEDOT:PSS electrodes

Porous polyurethane (PU) foams (Eurospuma, ref. 3049PR) were cut into cylindrical pieces using a Gunville foam cutter. Samples were washed with soap and distilled water, then sonicated for 10 min in acetone: distilled water (1:1, *v*/v), followed by drying with compressed air. Surface activation and hydrophilization were achieved by oxygen plasma treatment (Diener Atto, 40 kHz, 200 W, 10 min). The PEDOT:PSS coating solution was prepared by mixing 19 mL Clevios PH1000 (Heraeus Precious Metals GmbH & Co., 94.25 vol%) with 3-glycidyloxypropyltrimethoxysilane (GOPS) purchased from Sigma-Aldrich at 0.4% (*v*/v, 80 μL per 19 mL) and 1 mL of 5% (*v*/v) dimethyl sulfoxide (DMSO; Sigma-Aldrich). The dispersion was stirred for 6 h at room temperature. PU cylinders underwent four successive dip-coating cycles in the PEDOT:PSS mixture to achieve a conductive yet porous coating. For the first cycle, pristine PU was immersed overnight on an orbital shaker (200 rpm). After each cycle, samples were baked at 120 °C for 1 h in a muffle oven; during the first 20 min of each bake, the samples were rotated slowly, at 0.4 rpm, to ensure uniform distribution as in previous works [10,13].

For current collection, a circular Au pad with 10.7 mm^2, was fabricated by thermal evaporation (Edwards High Vacuum 4P) of Ti (10 nm) / Au (50 nm) onto a 2 mm-thick soda lime glass slide (Präzisions Glas & Optik GmbH). During the fourth dip-coating cycle, the PEDOT:PSS-coated PU cylinder was positioned directly onto the Au pad to form a porous PEDOT:PSS anode integrated with the Au pad collector [13].

2.2. Calculation of PU/PEDOT:PSS electrode area, volume and capacitance

The geometrical dimensions of PU/PEDOT:PSS electrodes (height 10.56 mm, diameter 4.94 mm, porosity 53.42%, PEDOT:PSS density 1 g/cm^3, Brunauer-Emmett-Teller or BET surface area 2.83 m^2/g, volumetric capacitance 21 F/cm^3) were used to estimate electrode surface area and capacitance. The external surface area was calculated assuming a cylinder with lateral area $A_{side} = 2\pi rh$ and base area $A_{base} = 2\pi r^2$, yielding $A_{external} = A_{side} + A_{base} = 2.022\ cm^2$.

The internal surface area was calculated as $A_{internal} = BET\ Surface\ Area\ (BSA) \times m$=0.03546 m^2 = 354.600 cm^2. Thus, $A_{total} = A_{external} + A_{internal} = 356.6\ cm^2$.

The total capacitance was determined using the volumetric capacitance $C_{vol} = 21F/cm^3$:

$$C_{total} = 21\frac{F}{cm^3} \times 0.01253 cm^3 = 0.2631\ F \quad (1)$$

The specific areal capacitance was:

$$C_{areal} = \frac{0.2631\ F}{354.6\ cm^2} = 7.42 \times 10^{-4}\ F \Big/ cm^2 = 0.742\ mF \Big/ cm^2 \quad (2)$$

2.3. Cyanobacterial culture, chlorophyll a extraction and cell-density calibration

The filamentous cyanobacterium *Oscillatoria* sp. UHCC 0332 was obtained from the HAMBI culture collection (University of Helsinki, Finland; http://www.helsinki.fi/hambi). This strain was chosen because its collection file reports production of the taste/odour compounds geosmin and 2-methylisoborneol (2-MIB), making it a relevant model for both biotechnological and environmental applications. Geosmin and 2-MIB are responsible for a significant number of poor water quality events globally every year requiring expensive removal in the water treatment works using ozone and activated carbon filtration. The *Oscillatoria* sp. was initially cultivated in BG11 in Erlenmeyer flasks under controlled conditions e.g., 30 μmol m^{-2} s^{-1}, cool-white light, 12 h:12 h photoperiod, 18 °C. Then, biomass was fragmented with a sterile scalpel, calibrated and inoculated on the electrodes. For calibration, 0.5 mL of filament suspension with high, medium and low concentration of filaments(n = 3 each) were extracted twice with cold 100% methanol (total 3.0 mL), incubated 1 h at 4 °C in the dark with occasional agitation, clarified with 4500 rpm for 10 min (2×), and the supernatant absorbance measured at 665 nm with Lan Optics V-1100 spectrophotometer. Chlorophyll *a* concentration was computed using a methanol equation (see Ritchie for solvent-specific coefficients) [14]:

$$Chl\ a\left(\mu g \bullet mL^{-1}\right) = k_{MeOH} \times A_{665} \quad (3)$$

where k_{MeOH}=12.95 is the calibrated coefficient [15], and A_{665} the absorbance at 665 nm measured in the methanol extract.

The Chlorophyll *a* concentration was then normalized to wet mass:

$$Chl\ a\left(\mu g \bullet g_{ww}^{-1}\right) = \frac{Chl\ a\left(\mu g \bullet mL^{-1}\right) \times V_{ext}}{m_{ww}} \quad (4)$$

where $Chl\ a\left(\mu g \bullet g_{ww}^{-1}\right)$ is the Chlorophyll *a* content normalized to wet biomass weight, V_{ext}=3.0 mL the total extraction volume used to extract pigments from the biomass and m_{ww} the wet weight of the biomass sample used for extraction.

To convert pigment data into cell density, we established a calibration curve by pairing chlorophyll *a* measurements with the average chlorophyll content reported for cyanobacteria (4.5 pg per cell [16]). This yielded approximate values of 1.0 × 10 [7], 3.9 × 10 [6], and 4.4 × 10^5 cells/mL for high, medium, and low density filament suspensions, respectively. For clarity, in this study we refer to these densities simply as 10 [7], 10 [6], and 10^5 cells/mL. This normalization across a range of concentrations avoids the limitations of simple chlorophyll-based estimations, which vary with species and physiological state, including light, nutrient availability, and growth phase [15,17,18].

The spatial evolution of extracellular polymeric substances (EPS) within the porous electrodes was qualitatively assessed by Alcian Blue staining. *Oscillatoria* sp. was cultivated on porous PU/PEDOT:PSS electrodes at an initial density of 1 × 10^7 cells/mL under standard growth conditions. At selected time points (day 0, 5, 10, 15 and 20), 20 μL of Alcian Blue solution (0.1% *w/v* in acetic acid, pH 2.5; Bio-Optica) was applied to the electrode surface for 10 min. Stained biofilms were then imaged directly within the porous scaffold using an inverted optical microscope (Zeiss Vert.A1).

2.4. Chronoamperometry

Chronoamperometry measurements were performed using porous PU/PEDOT:PSS working electrodes in a three-electrode configuration, with a platinum mesh counter electrode and an Ag/AgCl reference electrode. The working electrode active area was ~357 cm^2, with ~70% illuminated.

Electrodes were submerged in either sterile BG11 medium or BG11 inoculated with *Oscillatoria* sp. cultures. Light excitation was applied with an LED array delivering 270 $\mu mol\, m^{-2}s^{-1}$ of photosynthetically active radiation within 400–700 nm, unless otherwise stated in the text or supplementary section. Illumination consisted of 10 pulses of ~120 s duration, separated by ~120 s dark intervals. Photocurrent transients were recorded over ~4000 s, and plateau current values were extracted from the end of each light pulse after baseline subtraction.

2.5. OCP measurements and data extraction

Open-circuit potential (OCP) was recorded with a Keysight DAQ970A/DAQ973A Data Acquisition System equipped with three 20-channel multiplexer cards. A high-impedance differential voltage mode minimized cell loading. OCP was defined as the potential difference between the porous PU/PEDOT:PSS anode and the Au pad collector (cathode).

The DAQ sequentially scanned all channels at 600 s per channel, e.g., 10 min resolution, yielding synchronized long-term OCP traces across replicates. Temperature was simultaneously logged using a thermocouple (XF-1230-FAR) purchased from Labfacility and placed near the electrodes. Time-stamped data were exported as CSV and analysed in MATLAB.

OCP traces were reported as positive when the anode was at higher potential than the cathode. For temperature trend analysis, OCP data were optionally high-pass filtered with a 24 h centred moving average to preserve diurnal components while removing long-term drift. OCP data is expressed in millivolts and temperature in °C.

Schematic illustrations were created using Blender 3.4.

3. Results and discussion

3.1. Electrode colonization establishes a photosynthetic biohybrid and light-driven voltage responses

Porous PU/PEDOT:PSS electrodes served as the anode platform for biohybrid interfacing with *Oscillatoria* sp., as illustrated in Fig. 1A. SEM

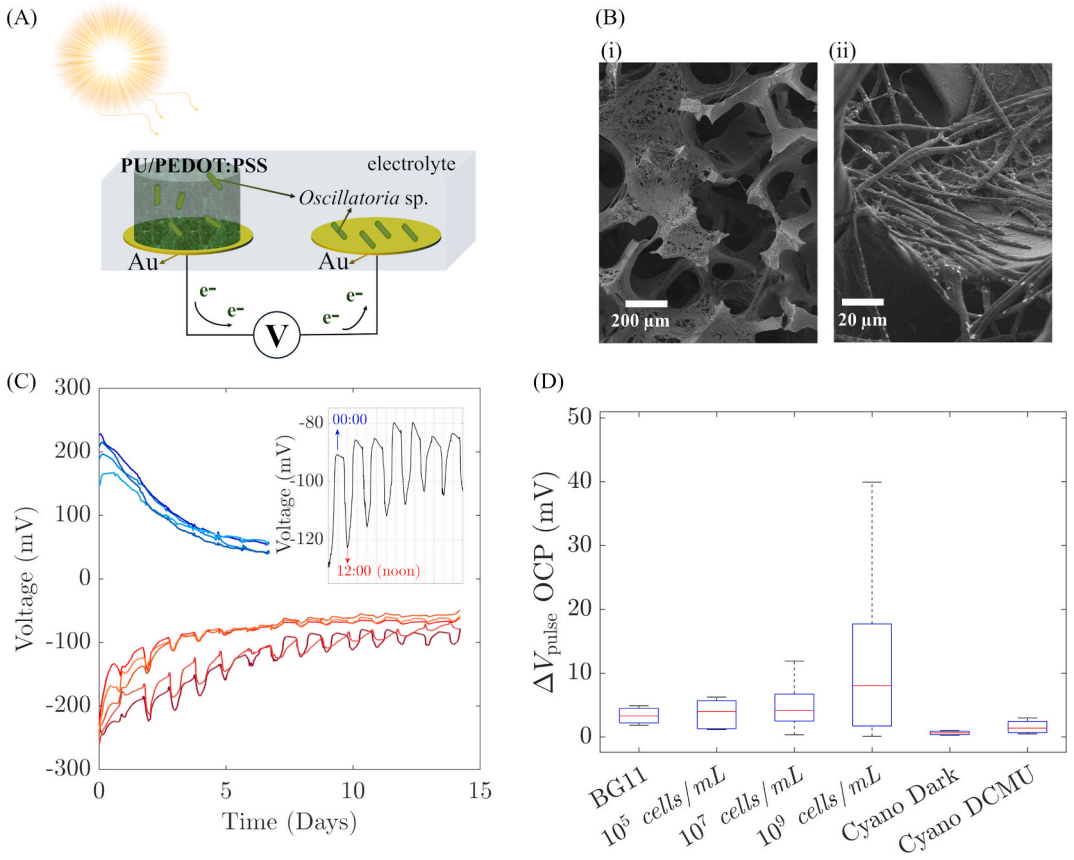

Fig. 1. Colonization of porous PEDOT:PSS electrodes and light-driven voltage responses. (A) Schematic of the two-electrode configuration used for open-circuit potential (OCP) monitoring. The working electrode consists of a porous PU/PEDOT:PSS foam supported on a circular Au collector pad and colonized by filaments of *Oscillatoria* sp. A second Au pad immersed in electrolyte serves as the counter/reference electrode. The potential difference between the PU/PEDOT:PSS and Au collectors is continuously recorded under diurnal light-dark cycles. (B) SEM micrographs of the porous foam with adherent *Oscillatoria* filaments: (i) macro view showing coverage of the porous architecture, and (ii) higher magnification of filaments interwoven across pores. (C) Representative OCP time traces over ~15 days for medium-only controls (blue traces) and cyanobacteria-inoculated electrodes (red traces). Clear diurnal oscillations driven by environmental light cycling are evident; Inset shows a 24-h window with midnight (00:00) and noon (12:00) indicated. (D) Box-and-whisker summary of the pulse amplitude at OCP, ΔV_{pulse} (mV), calculated as the peak-to-peak voltage oscillation between midnight and noon, for BG11 controls and electrodes inoculated with 10 [5], 10 [6], and 10^7 cells/mL of *Oscillatoria* sp., together with ΔV_{pulse} values recorded in dark conditions and under the photosystem II inhibitor DCMU (10 µM). Boxes show the interquartile range, the central line is the median, and whiskers indicate the full data range, excluding outliers. Responses remain close to controls at lower inoculation levels but become more distinct at higher cell densities, while dark and DCMU treatments markedly suppress the signal, consistent with a photosynthetically driven contribution. (For interpretation of the references to colour in this figure legend, the reader is referred to the web version of this article.)

imaging confirmed the highly porous structure of the electrode which provides an ultra-large interfacial area for electrochemical coupling. After incubation, *Oscillatoria* filaments adhered to and colonized the porous network as observed by the SEM micrographs in Fig. 1B i-ii, establishing intimate bioelectronic contact.

In the absence of cells, porous PEDOT:PSS electrodes behaved as light-sensitive interfacial capacitors, showing small millivolt-scale shifts under alternating light-dark conditions (see Fig. 1C, in blue). These responses likely arise from the large double-layer capacitance of the porous structure, combined with light absorption and local heating effects. PEDOT:PSS is not a classical photoactive semiconductor, but illumination can transiently excite polarons or bipolarons within PEDOT, altering local oxidation states, shifting the Fermi level, and reorganizing the electric double layer. The high porosity of the PU/PEDOT:PSS structure enhances these effects by enabling deep light penetration and slow relaxation. Dissolved O_2 and other redox-active species in BG11 may also contribute to minor background fluctuations [19,20].

When *Oscillatoria* sp. colonized the electrodes, the voltage response changed dramatically as shown in Fig. 1C, in red. In addition to baseline capacitive shifts, colonized electrodes displayed pronounced, pulse-like oscillations under diurnal illumination. Interestingly the diurnal patterns were not dissimilar to those for species-specific productivity data obtained through fluorescence monitoring on mixed algal and cyanobacterial communities [21]. Quantification of voltage pulse amplitudes (ΔV_{pulse}) confirmed significantly larger signals compared to BG11 controls, with medians of ~8 mV and maxima up to 40 mV. Also, in Fig. 1D, box-and-whisker analysis of ΔV_{pulse} shows that BG11 controls remained at low, narrowly distributed values with median = 2.5 mV and Interquartile Range (IQR) = 1.5–3.5 mV over $n = 5$. At low cell densities, within 10 [5]–10^6 cells/mL, the median response was slightly elevated, around 3–4 mV, but overlapping with controls. At 10^7 cells/mL, a clearer separation emerged, with median ΔV_{pulse} around 8 mV and maxima up to 40 mV with $n = 6$.

In contrast, ΔV_{pulse} was strongly suppressed in dark conditions (see Fig. S1) or with the PSII inhibitor DCMU, with $\Delta V_{pulse} < 1$ mV across all replicates, $n = 4$. In darkness or in the presence of the PSII inhibitor DCMU, ΔV_{pulse} was suppressed by 75–95%, confirming that the enhanced oscillations originated from photosynthetic activity. These trends indicate that measurable biohybrid responses become increasingly pronounced with higher cyanobacterial coverage, while optimization of electrode design and signal processing will be required to extend robust detection to lower densities.

The mechanism is consistent with PSII-driven water oxidation producing O_2 that accumulates within the biofilm and diffuses into the porous PEDOT:PSS network. Oxygen reduction reactions (ORR) at the polymer-electrolyte interface withdraw electrons from PEDOT:PSS, oxidizing the polymer and shifting the local mixed potential toward more positive values. We propose that the observed OCP dynamics reflect the interplay of two coupled contributions: (i) oxygen-dependent mixed-potential effects (O_2 accumulation/transport and ORR-driven polymer oxidation), which bias the potential positive, and (ii) photosynthesis-dependent redox coupling via reducing equivalents (mediated and eventually contact-based), which can modulate the polymer redox state in the opposite direction. Under illumination, the net response reflects the balance between these processes, while in darkness or upon PSII inhibition (DCMU) the photosynthesis-dependent contribution collapses and the signal relaxes toward baseline. In dark or low-light periods, the cessation of photosynthetic activity together with oxygen consumption and interfacial redox equilibration becomes dominant, driving the potential back toward its baseline value.

In cyanobacteria, alternative photosynthetic and respiratory electron pathways, including cyclic electron transport around PSI and oxygen-consuming reactions, can reduce local O_2 accumulation and limit net extracellular electron availability. These processes would both decrease net interfacial reducing equivalents and contribute to the reduced amplitude and transient character of the OCP signals observed when cyanobacteria are adhered to the electrodes [22].

While the strongest responses were obtained at higher inoculation densities, the presence of measurable shifts even at lower cell numbers suggests that with further optimization the platform could be adapted for earlier-stage or lower-density detection. We further note the small gradual decrease in OCP oscillation amplitude observed over prolonged cultivation does not necessarily indicate reduced photosynthetic activity. Optical microscopy and EPS staining (see Fig. S2) reveal progressive biofilm thickening and pore filling over time, which are expected to increase diffusion resistance and capacitive buffering at the biofilm-electrode interface. These structural changes can attenuate the magnitude of electrochemical transients sensed by the electrode, even under sustained photosynthetic conditions. Thus, signal amplitude reflects not only biological activity but also the evolving efficiency of bioelectronic coupling.

Owing to the large volumetric capacitance of porous PU/PEDOT:PSS electrodes and their ability to undergo redox changes throughout its structure, PU/PEDOT:PSS electrodes report both abiotic light- and temperature-sensitive capacitive signals and superimposed biologically driven photo-oscillations arising from cyanobacterial photosynthesis. These thermo-chemical influences add to the biological oscillations and are disentangled in section 3.2.

3.2. Cyano-mediated voltage rhythms are mostly light-driven, with residual temperature dependence

3.2.1. Theoretical background: Expected temperature effects

In bare Au electrodes submerged in BG11 medium, OCP shifts are expected to follow classical electrochemistry [23]. The mixed potential is governed by the Nernst equation for oxygen reduction:

$$E = E^0 - \frac{RT}{nF} ln\left(\frac{a_{red}}{a_{ox}}\right) \tag{5}$$

where, E is the electrode potential (V), E^0 is the standard reduction potential (V), R is the universal gas constant (8.314 $J{\cdot}mol^{-1}{\cdot}K^{-1}$), T is the absolute temperature (K), n is the number of electrons transferred in the redox reaction, F is the Faraday constant (96,485$C{\cdot}mol^{-1}$), a_{red} a_{ox} are the effective concentrations of the reduced and oxidized species, respectively.

Since the $\frac{RT}{nF}$ term grows with temperature, each °C rise produces a shift of a few tenths of a millivolt. In addition, dissolved oxygen (DO) solubility decreases by ~2%/°C[24], reducing the availability of O_2 for cathodic reactions. Together with the intrinsic temperature coefficient of the Ag/AgCl reference electrode, of about 0.7 mV/°C, this yields an expected drift of approximately 1 mV/°C, consistent with our Au electrode controls (data not shown). Also, porous PU/PEDOT:PSS electrodes in BG11-only displayed much larger sensitivity, with OCP shifts within 4–10 mV/°C. This amplification reflects the polymer's ultra-large interfacial area and volumetric redox activity, which magnify small changes in dissolved O_2 and redox equilibria into measurable voltage shifts.

3.2.2. Cross-correlation between voltage and temperature

To quantify the relationship between electrode potential and ambient temperature, we compared the detrended signals using the normalized cross-correlation function:

$$r(\tau) = Corr[v(t)\,, Temp(t+\tau)\,] = \frac{\sum_t [v(t) - \bar{v}][Temp(t+\tau) - \overline{Temp}\,]}{\sqrt{\sum_t [v(t) - \bar{v}]^2 \sum_t [Temp(t+\tau) - \overline{Temp}\,]^2}} \tag{6}$$

where $\bar{v}$ and $\overline{Temp}$ are the (time-averaged) means of the high-pass-filtered traces, and τ is calculated within [−48 h to +48 h]. From here we can calculate the lag, or time offset, by looking at values of τ where

$r(\tau)$ was largest. A peak in $r(\tau)$ at a given lag indicates that changes in temperature systematically precede or follow changes in electrode potential.

Fig. 2a shows representative normalized traces of OCP (black) and temperature (red). For BG11-only electrodes, correlation peaked at a lag of 0.47 h (Fig. 2c), confirming that their oscillations are largely driven by ambient heating and cooling. In cyanobacteria-colonized electrodes, cross-correlation revealed a longer lag of 2.17 h (Fig. 2b), consistent with a biological process that follows, but is not dictated by, temperature fluctuations (see also Fig. S3 showing the raw unprocessed temperature variations over time).

3.2.3. *Kinetic analysis of heating and cooling*

To extract characteristic time constants, individual voltage cycles were fitted to exponential rise and decay models. The voltage rise due to increase in temperature as a function of time, $V_{heating}(t)$ can be extracted as:

$$V_{heating}(t) = A\left[1 - e^{-(t-t_0)/\tau_{heating}}\right] \quad (7)$$

where t_0 is the time of cycle start, which is the local minimum temperature. On the other hand, when temperature decreases, the $V_{cooling}(t)$ is calculated based on:

$$V_{cooling}(t) = A\left[1 - e^{-(t-t_0)/\tau_{cooling}}\right] \quad (8)$$

For cyano-colonized electrodes, $\tau_{heating} = 4.64 \pm 2.80\ h$ and $\tau_{cooling} = 9.99 \pm 0.01\ h$ (Fig. 2d). In BG11-only controls, heating was slower ($14.30 \pm 3.60\ h$) and cooling faster ($6.34 \pm 3.25\ h$).

We argue that during warming, faster voltage rise in cyanobacteria-colonized electrodes reflects increased membrane fluidity, accelerated enzyme activity, and polymer reconfiguration that enhance electron transfer. Cooling is slower, requiring gradual lipid reordering, protein complex deactivation, and polymer relaxation, which collectively delay the return to baseline.

Thus, these findings indicate that temperature governs baseline drifts and modulates kinetics, but photosynthetic activity dominates the oscillatory voltage signals in cyanobacteria-PU/PEDOT:PSS electrodes hereafter referred to as biohybrids. The combination of cross-correlation lags and heating/cooling constants provides a quantitative fingerprint of living biohybrid electrochemistry.

4. Photocurrent responses indicate light-dependent faradaic currents

To further probe the functionality of the biohybrid, we performed chronoamperometry under repeated light-dark cycles. Fig. 3 illustrates the transient photocurrent responses measured on porous PU/PEDOT:PSS electrodes (357 cm^2 active area) under illumination with light pulses of ~120 s duration at a photosynthetic photon flux density (PPFD) of 270 $\mu mol\ photons\ m^{-2}s^{-1}$.

In BG11-only controls, the response was dominated by sharp capacitive spikes at each light-on event, followed by rapid decay back to baseline. This behaviour reflects the photoelectrochemical charging and discharging of the polymer's double-layer capacitance without sustained faradaic current. The charge per light-on event estimated in Eq. 9 was minimal, confirming the absence of biological electron flux.

$$Q = \int_0^{\infty} \Delta I \bullet e^{-t/\tau} dt = \Delta I \bullet \tau \quad (9)$$

When *Oscillatoria* sp. colonized the electrodes, the response changed markedly. Each light pulse produced a large, sustained photocurrent plateau with smooth rise and decay kinetics, well beyond the transient

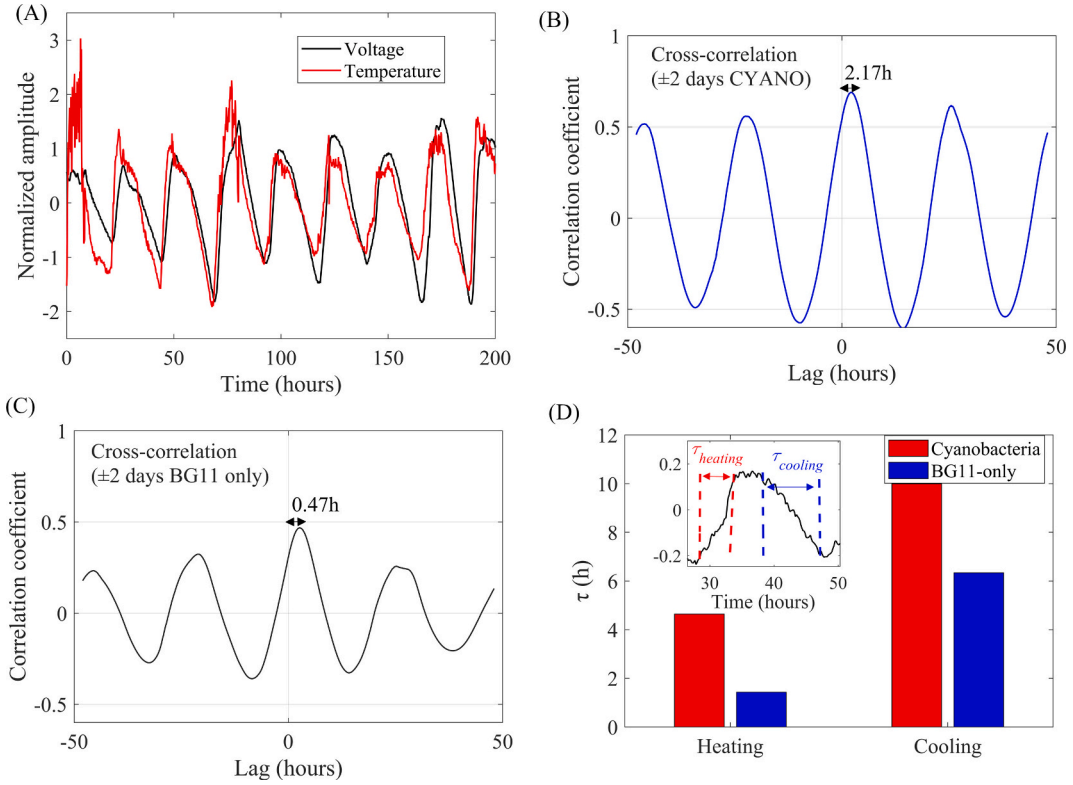

Fig. 2. Temperature dependence of open-circuit potential (OCP) oscillations in cyanobacteria-colonized electrodes. Measured electrochemical potential as a function of temperature. (A) Time lag for the high-passed filtered voltage (in black) and temperature signals (in red) with a one-day moving average removed and normalized to zero mean variance and overlaid on the same time axis. (B) Normalized cross-correlation, or Pearson correlation coefficient, between the detrended voltage $v(t)$ and temperature with cyanobacteria and (C) with BG11-only. (d) Heating and cooling times comparison with (red) and without (blue) cyanobacteria *Oscillatoria* sp. (For interpretation of the references to colour in this figure legend, the reader is referred to the web version of this article.)

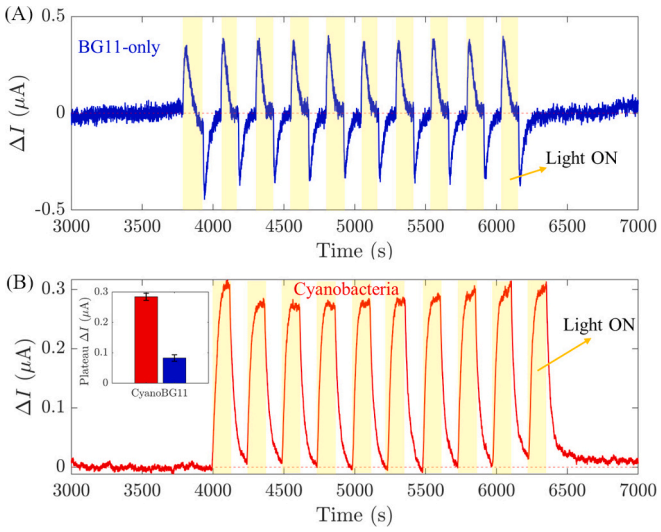

Fig. 3. - Photocurrent transients of cyanobacteria/PEDOT:PSS biohybrids measured by light-pulse chronoamperometry. Chronoamperometry on PU/PEDOT: PSS electrodes exposed to 10 light pulses (transparent yellow bars, duration of ~120 s, light intensity of 270 $\mu mol\ m^{-2}s^{-1}$ on an estimated 70% illuminated area of a 357 cm^2 sized electrode). (A) BG11-only control electrodes display minimal photocurrent response upon illumination. (B) Electrodes colonized with *Oscillatoria* sp. show strong photocurrent transients and sustained plateaus during light exposure. Inset shows the quantification of plateau photocurrent (ΔI) and highlights the significant contribution of photosynthetic activity. (For interpretation of the references to colour in this figure legend, the reader is referred to the web version of this article.)

capacitive spikes. Peak photocurrents reached 0.315 μA with a steady baseline above dark of 0.015 μA, giving a net Δ*I* of 0.300 μA. Over a 120 s light pulse, this corresponds to a delivered charge of ~36 μC, of which ~31 μC can be attributed to cyanobacteria after subtracting the BG11 contribution. Across 10 cycles, the average plateau photocurrent was 0.27 ± 0.01 μA, highly reproducible with <8% variation, consistent with robust light-driven redox coupling.

We note that in cyanobacteria, photosynthetic electrons are generated inside the thylakoid membranes, and for these electrons to reach the electrode without a mediator, they must traverse multiple barriers, including the thylakoid, cytoplasm, plasma membrane, and outer layers such. The fact that sustained photocurrents were detected indicates that biofilms formed on PEDOT:PSS enable efficient redox coupling with the electrode, potentially involving extracellular electron transfer through mediated and/or contact-based pathways.

Importantly, cross-correlation analysis showed that OCP oscillations tracked temperature cycles, but with distinct phase shifts and response times in cyanobacteria compared to medium, confirming a biological contribution beyond thermal effects. While electrodes in BG11-only medium responded nearly synchronously to daily temperature changes, electrodes colonized by *Oscillatoria* sp. exhibited a measurable lag of ~2 h. This behaviour suggests that the signal reflects cellular processes with slower kinetics rather than solely determined by abiotic temperature-redox coupling.

Several mechanisms may account for this delayed and phase-shifted response. First, the activity of photosynthetic and respiratory enzymes is temperature-dependent but not instantaneous, requiring time for activation or inhibition as the medium warms or cools. Second, oxygen produced during photosynthesis must accumulate within the biofilm and diffuse into the porous PEDOT:PSS network before participating in redox reactions, introducing an additional temporal offset relative to dissolved oxygen solubility changes in medium-only controls. Third, electrons generated within the thylakoid membranes must traverse multiple barriers, including cytoplasmic and plasma membranes as well as extracellular polysaccharide layers, before reaching the electrode, which may impose further kinetic delays. Finally, community-level behaviours such as circadian regulation or synchronized redox oscillations could also modulate the timing of electron release and the balance between linear and cyclic electron transport which is a function of ATP production and hence back pressure on the electron transport chain.

Together, these factors explain why cyanobacteria-covered electrodes do not follow temperature fluctuations with the same immediacy as abiotic controls. Instead, they produce a delayed but biologically informative signal, in which phase shifts reflect the combined influence of photosynthetic activity, biofilm architecture, and metabolic regulation.

Quantification further revealed that cyanobacteria enhanced photocurrent ~3.9-fold compared to BG11-only controls (0.27/0.07 μA), yielding an increase of ~286%. Normalized to the illuminated electrode area (~0.025 m^2, or 70% of 357 cm^2), the photocurrent density was 0.130 $\mu C \cdot cm^{-2}$ per 120 s pulse, confirming efficient, cell-dependent electron transfer into the polymer matrix. The ~70% of the total electrode area reflects the fact that the culture reservoir and experimental geometry did not permit full exposure of the electrode to incident light; approximately 30% of the surface area was shaded by the opaque chamber PEEK walls and support structures, leaving only ~70% directly illuminated.

The sustained currents in *Oscillatoria*-loaded electrodes are consistent with extracellular electron transfer (EET) processes. Photosynthetically generated electrons from PSII are passed through the intracellular transport chain and can reach the external PU/PEDOT:PSS interface either indirectly, via secreted redox mediators (e.g., quinones, phenazines, or other diffusible metabolites), or through redox-active proteins associated with the cell surface and extracellular matrix. In fact, directly supporting a photosynthetically driven mechanism, the photocurrent response is strongly suppressed upon addition of the PSII inhibitor DCMU, both in OCP and under chronoamperometric conditions (Fig. 1D and Supplementary Fig. S4). Further work could even employ techniques such as electrochemical impedance spectroscopy to better resolve diffusion-limited processes and interfacial resistances within the cyanobacterial biofilm and porous PEDOT:PSS network.

While *Oscillatoria* sp. does not produce conductive pili like certain electrogenic bacteria, its dense biofilm and extracellular layers create a close physical and chemical coupling with the electrode, enabling electron transfer to occur across the cell-polymer interface. In contrast, BG11-only controls lack this biological redox input and thus display only transient charging spikes. The detection of *Oscillatoria* sp. therefore reflects live biofilm-mediated electron transfer, likely reinforced by community-level interactions within the cyanobacterial network. Metabolic activity alters the local redox balance through continuous production and consumption of reactive metabolites, while extracellular electron transfer pathways channel photosynthetic electrons from the cells into the PEDOT:PSS matrix. Secreted redox-active compounds and direct cell-electrode contacts both contribute to the sustained faradaic currents observed. Together, these processes account for the combination of fast capacitive transients and slower, biologically driven photocurrents, firmly establishing PU/PEDOT:PSS as a sensitive bioelectronic interface for harvesting photosynthetic activity.

4.1. Proposed mechanism of light-driven electrochemical coupling at the cyanobacteria-PEDOT:PSS interface

Fig. 4 summarizes a conceptual model describing how photosynthetic activity in *Oscillatoria* sp. biofilms modulates the electrochemical response of porous PEDOT:PSS electrodes under light-dark cycling. Under illumination (e.g., Light ON), photosynthetic water oxidation at PSII produces molecular oxygen, which accumulates within the biofilm and diffuses into the porous PEDOT:PSS network. Oxygen reduction reactions (ORR) at the polymer-electrolyte interface withdraw electrons from PEDOT:PSS, driving polymer oxidation and shifting the local mixed potential. Owing to the mixed ionic-electronic conductivity and

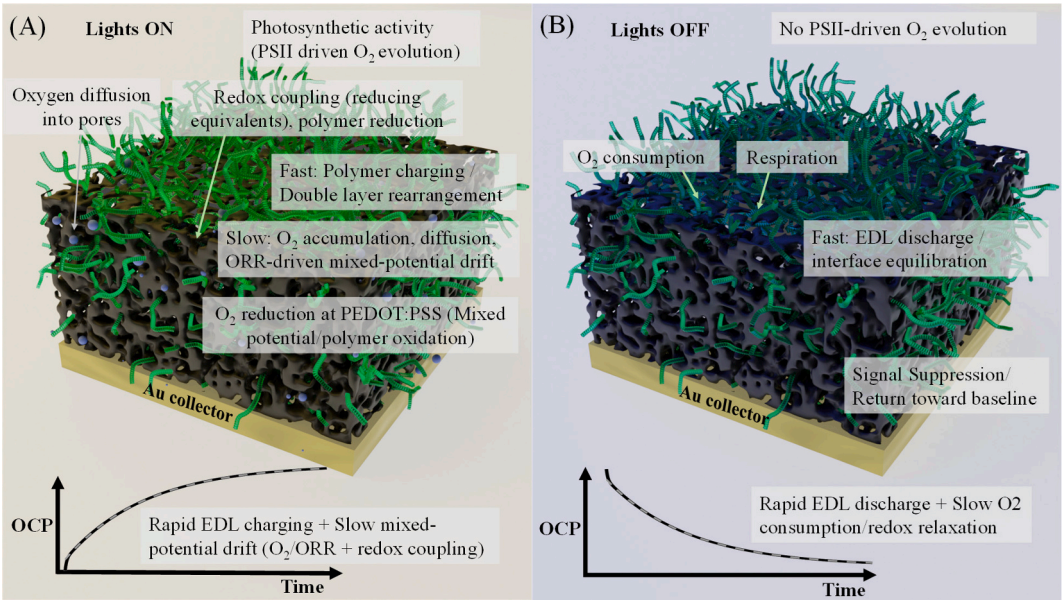

Fig. 4. - Conceptual model of light-dependent electrochemical coupling in cyanobacteria/PEDOT:PSS biohybrids. (A) Lights ON scenario. Photosynthetic activity in *Oscillatoria* sp. drives PSII-mediated O_2 evolution, leading to oxygen diffusion into the porous PEDOT:PSS electrode. Fast interfacial charging and electric double-layer (EDL) rearrangement dominate the immediate response to illumination, while slower oxygen accumulation, diffusion, and oxygen reduction reactions (ORR) modulate the local mixed potential and polymer redox state. In parallel, photosynthesis-derived reducing equivalents may contribute to polymer redox modulation through extracellular redox coupling pathways. The combined action of these processes produces sustained OCP shifts and photocurrent plateaus. (B) Lights OFF scenario. Upon cessation of illumination, PSII-driven O_2 evolution stops and dark respiration and net oxygen consumption dominate. A rapid EDL discharge and interfacial equilibration is followed by slower oxygen depletion and redox relaxation within the biofilm-polymer matrix, resulting in signal suppression and return toward baseline. Bottom panels schematically depict the corresponding fast and slow OCP components.

large volumetric capacitance of PEDOT:PSS[13], these redox processes are transduced into measurable changes in open-circuit potential (OCP) and sustained photocurrent plateaus. The immediate response to light switching is dominated by a fast interfacial process, attributed to electric double-layer (EDL) rearrangement and polymer charging, while slower dynamics reflect oxygen accumulation, diffusion and redox equilibration within the biofilm-electrode matrix.

In parallel, photosynthetically generated reducing equivalents may also influence the polymer through extracellular redox coupling pathways that are not mutually exclusive. These include mediated processes involving diffusible redox-active metabolites, as well as surface-associated or contact-based interactions between *Oscillatoria* sp. cells, extracellular matrices and the polymer surface. Such pathways would contribute to polymer reduction and partially counterbalance oxygen-driven oxidation, further modulating the mixed potential at the interface. The strong suppression of both OCP oscillations and photocurrent responses upon PSII inhibition with DCMU, or in the absence of illumination, supports a photosynthesis-dependent contribution to these electrochemical dynamics.

Upon cessation of illumination (e.g., Light OFF), PSII-driven oxygen evolution stops and dark respiration and net oxygen consumption dominate. The immediate electrochemical response is characterized by a rapid discharge of the EDL and interfacial equilibration with reversed polarity relative to light onset. This is followed by a slower relaxation governed by oxygen depletion, respiratory activity and gradual redox equilibration within the polymer and biofilm, resulting in signal attenuation and return of the OCP toward its baseline value.

Overall, the observed electrochemical response arises from the superposition of fast capacitive processes and slower biologically driven redox mechanisms. The model accounts for the measured phase shifts, latency relative to abiotic controls and coexistence of rapid transients with sustained signals. We note Fig. 4 is intended as a conceptual summary of these coupled processes and does not assume a single exclusive extracellular electron transfer pathway.

5. Conclusions

We have established a photosynthetic biohybrid that couples cyanobacteria with porous PEDOT:PSS electrodes for real-time monitoring of photosynthetic activity. Colonization of the porous polymer by *Oscillatoria* sp. enabled stable coupling of photosynthetically driven redox processes to the electrode. OCP monitoring revealed rhythmic diurnal light-dark oscillations, while chronoamperometry confirmed light-driven electron transfer into the electrode. Temperature analysis further distinguished biological activity from abiotic artifacts, demonstrating that the observed signals arise from coupled biological and physicochemical processes. By integrating light-driven responses with temperature-dependent dynamics, this biohybrid platform provides a non-invasive, label-free approach to monitor cyanobacterial productivity, underscoring its potential for environmental monitoring alongside applications in algal biotechnology and bioenergy. We note that signal amplitude reflects both biological activity and the evolving efficiency of biofilm-electrode coupling, emphasizing the importance of structural context in long-term monitoring. Nevertheless, the system detects biological activity at cell densities on the order of 10^7 cells/mL corresponding to dense bloom conditions reported in the literature, underscoring its potential relevance for environmental monitoring.

CRediT authorship contribution statement

Paulo R.F. Rocha: Writing – review & editing, Writing – original draft, Visualization, Resources, Project administration, Methodology, Investigation, Funding acquisition, Formal analysis, Data curation, Conceptualization. **Raquel Amaral:** Methodology, Investigation. **David M.S. Silva:** Methodology, Investigation. **Felipe L. Bacellar:** Data curation, Formal analysis, Investigation, Methodology. **Luís Lopes:** Writing – review & editing, Methodology. **Rupert Perkins:** Writing – review & editing, Methodology, Investigation.

Declaration of competing interest

The authors declare the following financial interests/personal relationships which may be considered as potential competing interests: Paulo R.F. Rocha reports financial support was provided by European Commission. If there are other authors, they declare that they have no known competing financial interests or personal relationships that could have appeared to influence the work reported in this paper.

Acknowledgements

Paulo R.F. Rocha acknowledges the support and funding from the European Research Council (ERC) under the European Union's Horizon 2020 research and innovation programme (grant agreement No. 947897).

Appendix A. Supplementary data

Supplementary data to this article can be found online at https://doi.org/10.1016/j.bioelechem.2026.109261.

Data availability

Data will be made available on request.

References

[1] V.A. de Mescouto, et al., Review of recent advances in improvement strategies for biofuels production from cyanobacteria, Heliyon 10 (2024) e40293, https://doi.org/10.1016/j.heliyon.2024.e40293.
[2] R. Miao, et al., Engineering Cyanobacteria for biofuel production, in: P. C. Hallenbeck (Ed.), Modern Topics in the Phototrophic Prokaryotes: Environmental and Applied Aspects, Springer International Publishing, Cham, 2017, pp. 351–393, https://doi.org/10.1007/978-3-319-46261-5_11.
[3] J. Zhou, Y. Li, Engineering cyanobacteria for fuels and chemicals production, Protein Cell 1 (2010) 207–210, https://doi.org/10.1007/s13238-010-0043-9.
[4] I. Havlik, S. Beutel, T. Scheper, K.F. Reardon, On-line monitoring of biological parameters in microalgal bioprocesses using optical methods, Energies 15 (2022) 875, https://doi.org/10.3390/en15030875.
[5] I. Chorus, J. Bartram, Toxic Cyanobacteria in Water: A Guide to their Public Health Consequences, Monitoring and Management, CRC Press, 1999.
[6] T.J. Zajdel, et al., PEDOT:PSS-based multilayer bacterial-composite films for bioelectronics, Sci. Rep. 8 (2018) 15293, https://doi.org/10.1038/s41598-018-33521-9.
[7] A. Wang, D. Jung, D. Lee, H. Wang, Impedance characterization and modeling of subcellular to Micro-sized electrodes with varying materials and PEDOT:PSS coating for bioelectrical interfaces, ACS Appl. Electron. Mater. 3 (2021) 5226–5239, https://doi.org/10.1021/acsaelm.1c00687.
[8] S.K. Ravi, et al., Enhanced output from biohybrid photoelectrochemical transparent tandem cells integrating photosynthetic proteins genetically modified for expanded solar energy harvesting, Adv. Energy Mater. 7 (2017) 1601821, https://doi.org/10.1002/aenm.201601821.
[9] Y. Tokunou, et al., *Synechococcus* and other bloom-forming Cyanobacteria exhibit unique redox signatures, ChemElectroChem 8 (2021) 360–364, https://doi.org/10.1002/celc.202001274.
[10] F.C. Cotta, et al., Porous PU/PEDOT:PSS electrodes for probing bioelectricity in *Oscillatoria* sp. cohorts, Chem. Eng. J. 498 (2024) 155480, https://doi.org/10.1016/j.cej.2024.155480.
[11] K. Ha, H.W. Kim, G.J. Joo, The phytoplankton succession in the lower part of hypertrophic Nakdong River (Mulgum), South Korea, Hydrobiologia 369–370 (1998) 217–227, https://doi.org/10.1023/A:1017067809089.
[12] A. Aguilera, et al., Cyanobacterial bloom monitoring and assessment in Latin America, Harmful Algae 125 (2023) 102429, https://doi.org/10.1016/j.hal.2023.102429.
[13] F.C. Cotta, et al., A 3D porous electrode for real-time monitoring of microalgal growth and exopolysaccharides yields using electrochemical impedance spectroscopy, Biosens. Bioelectron. 277 (2025) 117260, https://doi.org/10.1016/j.bios.2025.117260.
[14] R.J. Ritchie, Consistent sets of spectrophotometric chlorophyll equations for acetone, methanol and ethanol solvents, Photosynth. Res. 89 (2006) 27–41, https://doi.org/10.1007/s11120-006-9065-9.
[15] R.J. Ritchie, Universal chlorophyll equations for estimating chlorophylls a, b, c, and d and total chlorophylls in natural assemblages of photosynthetic organisms using acetone, methanol, or ethanol solvents, Photosynthetica 46 (2008) 115–126, https://doi.org/10.1007/s11099-008-0019-7.
[16] S.B. Silveira, C. Odebrecht, Effects of light intensity and nutrients (N and P) on growth, toxin concentration, heterocyte formation and akinete germination of *Nodularia spumigena* (Cyanobacteria), Hydrobiologia 848 (2021) 4387–4400, https://doi.org/10.1007/s10750-021-04649-z.
[17] N.D. Wagner, et al., Diazotrophy modulates cyanobacteria stoichiometry through functional traits that determine bloom magnitude and toxin production, Limnol. Oceanogr. 68 (2023) 348–360, https://doi.org/10.1002/lno.12273.
[18] A.V. Volkov, et al., Understanding the capacitance of PEDOT:PSS, Adv. Funct. Mater. 27 (2017) 1700329, https://doi.org/10.1002/adfm.201700329.
[19] N. Calabia Gascón, H. Terryn, A. Hubin, The role of PEDOT:PSS in (super) capacitors: a review, Next Nanotechnol. 2 (2023) 100015, https://doi.org/10.1016/j.nxnano.2023.100015.
[20] J.F. Baez, et al., Controlling the mixed potential of polyelectrolyte-coated platinum electrodes for the potentiometric detection of hydrogen peroxide, Anal. Chim. Acta 1097 (2020) 204–213, https://doi.org/10.1016/j.aca.2019.11.018.
[21] G.J.C. Underwood, et al., Patterns in microphytobenthic primary productivity: species-specific variation in migratory rhythms and photosynthetic efficiency in mixed-species biofilms, Limnol. Oceanogr. 50 (2005) 755–767, https://doi.org/10.4319/lo.2005.50.3.0755.
[22] D.C. Ducat, J.C. Way, P.A. Silver, Engineering cyanobacteria to generate high-value products, Front. Plant Sci. 5 (2014) 7, https://doi.org/10.3389/fpls.2014.00007.
[23] P. Lasala, et al., Deciphering the role of inorganic nanoparticles' surface functionalization on biohybrid microbial Photoelectrodes, ACS Appl. Mater. Interfaces 16 (2024) 58598–58608, https://doi.org/10.1021/acsami.4c12070.